PCCP

PAPER

Cite this: *Phys. Chem. Chem. Phys.*, 2024, **26**, 11825

Adjustment of optical absorption in phosphorene through electron–phonon coupling and an electric field

Do C. Hap,[a] Le P. Q. Hung,[a] Luong T. Tung,[a] Le T. T. Phuong [a] and Tran Cong Phong *[bc]

Received 14th January 2024,
Accepted 18th March 2024

DOI: 10.1039/d4cp00167b

rsc.li/pccp

This study investigates the optical absorption of monolayer phosphorene, focusing on its response to the electron–phonon coupling (EPC) and an electric field. Using a tight-binding Hamiltonian model based on the Barišic–Labbe–Friedel–Su–Schrieffer–Heeger model and the Kubo formula, we calculate the electronic band structure and optical absorption characteristics. The anisotropic dispersion of carriers along armchair and zigzag directions leads to distinct optical responses. Positive and negative EPC effects increase and decrease hopping parameters, respectively, enlarging and reducing/closing the band gap. Moreover, both EPCs cause an admixture of blue and red shift spectrum along the armchair direction, while a red (blue) shift spectrum is observed for positive (negative) EPC along the zigzag direction. Incorporating electric field effects in the EPC increases band gaps for both positive and negative EPC activities, resulting in shifted optical peaks along both directions.

1 Introduction

The identification of graphene[1–3] has opened avenues for exploring the synthesis and fabrication of other two-dimensional (2D) materials, aiming to uncover novel physical properties in condensed matter systems. While graphene-based electronic devices face challenges due to graphene's zero band gap, resulting in a low on–off current ratio,[4,5] materials like silicene,[6] germanene,[7] and transition-metal dichalcogenides exhibit high on–off current ratios but suffer from low carrier mobilities, restricting their applications in optoelectronics.[8–10]

In addressing the challenges mentioned above, recent exploration of a 2D semiconductor has spotlighted phosphorene – a monolayer of phosphorus crystal. Phosphorene exhibits a high mobility for carriers and a tunable direct band gap.[11,12] The pronounced anisotropic behavior of high carrier mobilities in phosphorene results in a strongly anisotropic dispersion.[13–18] This characteristic, in turn, gives rise to significant anisotropic optical properties, positioning phosphorene as a promising candidate in optoelectronics.[19–22] Notably, the optical absorption spectra of phosphorene reveal a strong direction dependency in reality.[14,16,17] It has been experimentally proved that black phosphorus thin films show high mobility above 600 $cm^2 V^{-1} s^{-1}$ and 1000 $cm^2 V^{-1} s^{-1}$ at 120 K along the light (x) and heavy (y) effective mass directions, implying their promising future for high frequency, thin-film electronics, as well as great potential for infrared optoelectronics and novel devices in which anisotropic properties are desirable.[14] Moreover, it has been experimentally reported that the continuum absorption near the band edge in phosphorene is almost a constant, independent of the thickness, which is related to the quanta of the universal optical conductivity with a prefactor originating from the band anisotropy.[16] Also, the highly anisotropic nature of phosphorene has been demonstrated through Raman and polarization photoluminescence measurements.[17]

Considering the intriguing response exhibited by phosphorene in various orientations, despite theoretical first-principles studies on the optical properties of phosphorene under external fields,[23–28] there is a notable scarcity of analytical studies to date focusing on the microscopic behavior of phosphorene's optical absorption with the electron–phonon coupling (EPC) and electric field (EF).[29–31] In ref. 32, the highly anisotropic properties of phosphorene are explored, making it a compelling material for directional applications. Specifically, it addresses the interplay between strain and electric field stimuli in assessing the band gap and electron energy loss spectrum (EELS). The electric field induces a blueshift in interband optical transitions along the armchair direction, while in-plane/out-of-plane strain causes a red/blueshift. In ref. 33, the impact of strain on the optical refraction and absorption of monolayer

[a] *Faculty of Physics, University of Education, Hue University, Hue, 530000, Vietnam*
[b] *Atomic Molecular and Optical Physics Research Group, Institute for Advanced Study in Technology, Ton Duc Thang University, Ho Chi Minh City, Vietnam. E-mail: trancongphong@tdtu.edu.vn*
[c] *Faculty of Electrical and Electronics Engineering, Ton Duc Thang University, Ho Chi Minh City, Vietnam*

black phosphorus is calculated. The study highlights that variations in refraction inflections and absorption peaks are dependent on the strained band gap, and the influence of out-of-plane strains differs from in-plane strains. Moreover, it has been proposed that a Zeeman spin-splitting field can change the absorption spectrum at various frequencies of incident light[34] such that irregular (regular) processes for optical conductivity with the Zeeman field along the armchair (zigzag) direction result in irregular (regular) absorption and scattering mechanisms.

This study aims to adjust the interband optical absorption of single-layer phosphorene using a gate voltage for including the EF effects as well as a substrate for including the EPC effects. Although EPC can also be considered using the nonadiabatic molecular dynamics method when investigating the electron–hole recombination and interlayer charge transfer process,[35,36] we include it *via* the renormalization of the hopping energies. Indeed, the movement of atoms in the lattice affects the orbital hybridization of atoms in a material and eventually the electronic structure of the material. To achieve these, we employ the Hamiltonian model proposed in ref. 37–42 to calculate the electronic dispersion of carriers. Subsequently, the optical absorption along the armchair and zigzag directions is assessed using the Kubo formula.

The following sections of the paper are structured as follows: in Section 2, we present the Hamiltonian model and deduce the associated electronic band structure under the influence of the EPC and EF. The determination of optical absorption in phosphorene is outlined in Section 3. Moving forward, the results for both armchair and zigzag directions are presented and discussed in Section 4, and finally, we end the paper with a summary of notable findings in Section 5.

2 Tight-binding Hamiltonian model

Exploring the role of EPC and EF in phosphorene's optical absorption involves starting with the geometry arrangement of atoms in phosphorene to build the Hamiltonian model. Phosphorene's unit cell is composed of four phosphorus atoms distributed across two sublayers, each containing two atoms, illustrated in Fig. 1, and a four-band tight-binding model for nearest neighbor lattice sites up to the fifth neighbors yields the effective band structure around the Fermi level.[26,37–39,42] The symmetries exhibited by atoms in both sublayers of phosphorene allow for a reduction in the number of atoms within the unit cell from 4 to 2. Consequently, this leads to the formation of a new single-layer structure, featuring just two atoms within the unit cell. Much like graphene and other planar 2D materials, the out-of-plane (p_z or π) orbitals play a predominant role in electronic transport within such lattices. However, identical atoms on both sublayers lead to a two-band tight-binding model for effective responses of the momentum-dependent Hamiltonian for a one-orbital p_z-like configuration (confirmed through projected density of states),[37,43] given by $\mathscr{H} = \sum_{\ell} t_\ell c_\ell^\dagger c_{\ell+1}$. This pristine two-band model has been

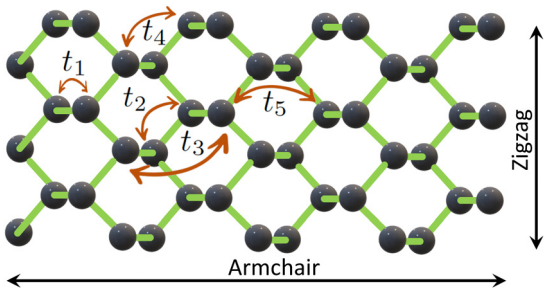

Fig. 1 Illustration of the top view of phosphorene is provided. The unit cell of phosphorene contains four phosphorus atoms in two sublayers with five hopping energies between atoms. While there may be additional hoppings present in reality, these five are the crucial ones necessary for accurately replicating the electronic band structure of phosphorene.

corroborated by first-principles studies. Furthermore, considering the introduction of electron–phonon coupling in the following through minor modulations of hopping parameters, we maintain that the two-band model remains valid for low-energy excitations. The summation ℓ considers all nearest neighbor lattice sites (sublayers), t_ℓ represents the hopping energy between atomic sites ℓ, and $c_\ell^\dagger$ and c_ℓ denote, respectively, the creation and annihilation operators for an electron at the ℓ-th atomic site of each sublayer. The expression for the effective two-band Hamiltonian $\mathscr{H}_{\vec{k}}$ in the reciprocal space is then provided as:[42]

$$\mathscr{H}_{\vec{k}} = \begin{pmatrix} f_{\vec{k}} & g_{\vec{k}} \\ g_{\vec{k}}^* & f_{\vec{k}} \end{pmatrix}, \tag{1}$$

where

$$f_{\vec{k}} = 4t_4 \cos(k_x a/2)\cos(k_y b/2), \tag{2a}$$

$$g_{\vec{k}} = 2t_1 e^{-ik_x a_{1x}} \cos(k_y b/2) + t_2 e^{ik_x a_{2x}} + 2t_3 e^{ik_x a_{3x}} \cos(k_y b/2) + t_5 e^{-ik_x a_{5x}}. \tag{2b}$$

Here, the momenta $\vec{k} = (k_x, k_y)$ are within the first Brillouin zone (FBZ) of phosphorene. In our model, we focus on five specific hopping energies: $t_1 = -1.220$ eV, $t_2 = +3.665$ eV, $t_3 = -0.205$ eV, $t_4 = -0.105$ eV, and $t_5 = -0.055$ eV,[26,37,38] as depicted in Fig. 1. Moreover, utilizing the symmetry properties between atoms in two distinct sublayers, we adapt parameters: $a_{1x} = 1.41763$ Å, $a_{2x} = 2.16400$ Å, $a_{3x} = 3.01227$ Å, $a_{4x} = 2.21468$ Å, and $a_{5x} = 3.63258$ Å from ref. 37, 38 and 42, denoting the distances between intra- and inter-planar nearest-neighbor atoms projected onto the x direction. Additionally, $a = 4.42936$ Å and $b = 3.27$ Å represent the lengths of the unit cell along the armchair and zigzag directions, respectively.

To investigate the electronic properties of carriers under a gate voltage influence (for including the EF effects), we install a gate voltage on both sublayers (considering the distance $d \approx 0.7$ nm[44] between them) with positive $+\Delta_z/2$ and negative $-\Delta_z/2$ potentials, respectively,[40,41,45] where $\Delta_z = eE_z d$ and $e(E_z)$ refers to the electron's charge (induced EF). This, in turn, induces a

mass term $(\Delta_z/2)\tau_z$ to the matrix representation of phosphorus atoms, where τ_z is the z-component of the Pauli matrix in the real space. Hence, the following EF-induced Hamiltonian is achieved:[37–39]

$$\mathscr{H}_{\vec{k}} = \begin{pmatrix} f_{\vec{k}} + \Delta_z/2 & g_{\vec{k}} \\ g^*_{\vec{k}} & f_{\vec{k}} - \Delta_z/2 \end{pmatrix}. \tag{3}$$

Turning to the EPC effect, we use the Barišic–Labbe–Friedel–Su–Schrieffer–Heeger model, which is a one-dimensional model used to describe the interaction between electrons and phonons in a crystal lattice.[46–50] This interaction is a central aspect of condensed matter physics and materials science, which needs to be considered in the study of electro-optical properties. As phonons can modify the distances between atoms, they influence the spatial distribution of electrons around atoms. Thus, the effective potential felt by electrons is altered, changing the overlap of atomic orbitals and affecting the degree of orbital hybridization, manifesting itself in the hopping parameters as[46–50]

$$\tilde{t}_\ell = t_\ell(1 - \tanh[G_1/|t_\ell|] - \tanh[G_2/|t_\ell|]). \tag{4}$$

It is important to note that electrons from both sublayers experience distinct potentials. As a result, G_1 and G_2 represent the effective EPCs governing the hopping parameters of the first and second sublayers, respectively. Nevertheless, these potentials cannot be excessively strong within the context of our low-energy model. Consequently, we have chosen to limit them to values less than 0.5 eV to ensure that their effects remain comparable with the model. The sign of the electron–phonon coupling can be positive or negative such that a positive EPC signifies that the presence of electrons enhances the lattice vibrations or phonons, leading to a positive contribution to the overall energy, while a negative coupling implies that the electrons tend to suppress or dampen the lattice vibrations, resulting in a negative contribution to the total energy. With this, the following Hamiltonian model in the presence of both EF and EPC is obtained:

$$\mathscr{H}_{\vec{k}} = \begin{pmatrix} \tilde{f}_{\vec{k}} + \Delta_z/2 & \tilde{g}_{\vec{k}} \\ \tilde{g}^*_{\vec{k}} & \tilde{f}_{\vec{k}} - \Delta_z/2 \end{pmatrix}, \tag{5}$$

where

$$\tilde{f}_{\vec{k}} = 4\tilde{t}_4 \cos(k_x a/2)\cos(k_y b/2), \tag{6a}$$

$$\tilde{g}_{\vec{k}} = 2\tilde{t}_1 e^{-ik_x a_{1x}}\cos(k_y b/2) + \tilde{t}_2 e^{ik_x a_{2x}} + 2\tilde{t}_3 e^{ik_x a_{3x}}\cos(k_y b/2) + \tilde{t}_5 e^{-ik_x a_{5x}}. \tag{6b}$$

By diagonalizing the Hamiltonian above, the energy dispersion of carriers is obtained as (for both valence (−) and conduction (+) bands)

$$\mathscr{E}_{\vec{k},\pm} = \tilde{f}_{\vec{k}} \pm \sqrt{\frac{\Delta_z^2}{4} + |\tilde{g}_{\vec{k}}|^2}. \tag{7}$$

3 Optical absorption

In this study, we utilize the Kubo formula to derive the optical absorption within the EPC- and EF-induced monolayer phosphorene.[51–53] Specifically, our focus is on understanding how such a system responds to an applied light field $\vec{E}(\omega)$. It is important to note that the system is undoped, indicating that the Kubo formula exclusively likes the interband contribution. Regarding intraband transition effects, another potential consideration, we argue that they also hold significance, particularly in scenarios where disorder or scattering of the host electrons in the THz region (exhibiting Drude-like conductivity) is under study. However, it is important to note that this aspect falls outside the scope of our current investigation. To reiterate, the non-interacting Hamiltonian in the reciprocal space is denoted as $\mathscr{H}_0 = \sum_{\vec{k},\pm} \mathscr{E}_{\vec{k},\pm} c^\dagger_{\vec{k},\pm} c_{\vec{k},\pm}$. The total Hamiltonian, which includes the interacting term in the presence of the light field, is expressed as $\mathscr{H} = \mathscr{H}_0 + \mathscr{H}_{\text{int}}$, where $\mathscr{H}_{\text{int}} = \vec{J}\cdot\vec{A}$. The vector potential $\vec{A}$ can be determined by the relationship $\vec{E}(\omega) = -\partial_t\vec{A}$, and the current density $\vec{J}$ along the direction $\alpha \in \{x,y\}$ is connected to the β components of the corresponding light field E_β in the linear response of the optical conductivity σ as $J_\alpha = \sigma_{\alpha\beta}E_\beta$.

To derive $\vec{J}$, it is necessary to have the wave functions of the total Hamiltonian $\mathscr{H}$ considering the wave vector $\vec{k} + (e/\hbar)\vec{A}$. Consequently, the calculation of the α-component of $\vec{J}$ is as follows:

$$J_\alpha = -\frac{e}{\hbar}\sum_{\vec{k},\pm} c^\dagger_{\vec{k},\pm} c_{\vec{k},\pm}\nu^\alpha_{\vec{k}} + i\frac{e}{\hbar}\sum_{\vec{k},\pm} c^\dagger_{\vec{k},\pm} c_{\vec{k},\mp}\chi^\alpha_{\vec{k}}. \tag{8}$$

The first (second) term is referred to as the paramagnetic (diamagnetic) term, and the quantities $\{V^\alpha_{\vec{k}}, \chi^\alpha_{\vec{k}}\}$ are linked to the carriers' velocity (the term $\chi^\alpha_{\vec{k}}$ means the dipole transition for interband transitions), as[42]

$$\begin{aligned}\nu^x_{\vec{k}} = {} & +2t_1 a_{1x}\sin\left(k_x a_{1x} + \theta_{\vec{k}}\right) + t_2 a_{2x}\sin\left(k_x a_{2x} - \theta_{\vec{k}}\right) \\ & + 2t_3 a_{3x}\cos\left(k_y b/2\right)\sin\left(k_x a_{3x} - \theta_{\vec{k}}\right) \\ & + 2t_4 a\sin(k_x a/2)\times\cos\left(k_y b/2\right) \\ & + t_5 a_{5x}\sin\left(k_x a_{5x} + \theta_{\vec{k}}\right),\end{aligned} \tag{9a}$$

$$\begin{aligned}\nu^y_{\vec{k}} = {} & +bt_1\sin\left(k_y b/2\right)\cos\left(k_x a_{1x} + \theta_{\vec{k}}\right) + bt_3\sin\left(k_y b/2\right) \\ & \times\cos\left(k_x a_{3x} + \theta_{\vec{k}}\right) + 2t_4 b\cos(k_x a/2)\sin\left(k_y b/2\right),\end{aligned} \tag{9b}$$

$$\begin{aligned}\chi^x_{\vec{k}} = {} & -2t_1 a_{1x}\cos\left(k_y b/2\right)\cos\left(k_x a_{1x} + \theta_{\vec{k}}\right) \\ & + t_2 a_{2x}\cos\left(k_x a_{2x} - \theta_{\vec{k}}\right) \\ & + 2t_3 a_{3x}\cos\left(k_y b/2\right)\cos\left(k_x a_{3x} - \theta_{\vec{k}}\right) \\ & - t_5 a_{5x}\cos\left(k_x a_{5x} + \theta_{\vec{k}}\right),\end{aligned} \tag{9c}$$

$$\chi_{\vec{k}}^{y} = +bt_1 \sin(k_y b/2) \sin(k_x a_{1x} + \theta_{\vec{k}}) - bt_3 \sin(k_y b/2) \times \sin(k_x a_{3x} - \theta_{\vec{k}}). \quad (9d)$$

where $g_{\vec{k}} = |g_{\vec{k}}| e^{i\theta_{\vec{k}}}$.

Ultimately, the optical conductivity normalized to the planar area is derived by:

$$\sigma_{\alpha\beta}(\omega) = \frac{2}{\hbar\omega}\int_0^{\infty} \mathrm{d}t e^{i\omega t} \langle [J_\alpha(t), J_\beta(0)] \rangle. \quad (10)$$

The factor of 2 accounts for spin degeneracy. As previously mentioned, our focus in this study is on interband optical transitions, assuming that the incident photons are sufficiently strong, leading to transitions from the valence to the conduction band. Due to the structural symmetry of phosphorene, the contributions of Hall conductivity are zero, *i.e.*, $\sigma_{xy}(\omega) = \sigma_{yx}(\omega) = 0$. As a result of this, the optical conductivity along the armchair (xx) or zigzag (yy) direction is then calculated as:

$$\frac{\sigma_{\alpha\alpha}(\omega)}{\sigma_0} = -\frac{4i}{\hbar\omega} \sum_{\vec{k}\in \mathrm{FBZ}} \left(\chi_{\vec{k}}^{\alpha}\right)^2 \frac{\left(n_{\vec{k},+}^{\mathrm{FD}} - n_{\vec{k},-}^{\mathrm{FD}}\right)\left(\mathscr{E}_{\vec{k},+} - \mathscr{E}_{\vec{k},-}\right)}{(\hbar\omega + i\eta)^2 - \left(\mathscr{E}_{\vec{k},+} - \mathscr{E}_{\vec{k},-}\right)^2}, \quad (11)$$

where the optical conductivity's universal value is denoted by $\sigma_0 = e^2/\hbar$, while $\eta = 10$ meV represents the finite damping between the valence and conduction bands. $n_{\vec{k},\pm}^{\mathrm{FD}} = \left(1 + \exp\left[\left(\mathscr{E}_{\vec{k},\pm} - \mu\right)\Big/\left(k_{\mathrm{B}}T\right)\right]\right)^{-1}$, with k_{B} being the Boltzmann constant, expresses the Fermi–Dirac distribution function at μ (chemical potential) and T (absolute temperature).

Now, we proceed to compute the absorption spectra. Initially, we establish the connection between the optical conductivity and the dielectric function, as expressed by:

$$\varepsilon_{\alpha\alpha}(\omega) = \varepsilon_{\mathrm{r}} + i\frac{\sigma_{\alpha\alpha}(\omega)}{\omega\varepsilon_0 d}, \quad (12)$$

where $\varepsilon_{\mathrm{r}}(\varepsilon_0)$ represents the relative (vacuum) permittivity of phosphorene. Following this, we determine the extinction coefficient by utilizing the real and imaginary components of the dielectric function through:

$$\kappa_{\alpha\alpha}{}^2(\omega) = \frac{|\varepsilon_{\alpha\alpha}(\omega)| - \mathrm{Re}[\varepsilon_{\alpha\alpha}(\omega)]}{2}. \quad (13)$$

Lastly, taking into account the speed of light c during the absorption process in phosphorene, the optical absorption is obtained as:

$$\text{Optical absorption} = \frac{2\hbar\kappa_{\alpha\alpha}(\omega)}{c}. \quad (14)$$

4 Results

The role of gate voltage (electric field) effects has been extensively explored in prior research, as evidenced by ref. 25, 32, 37–41 and 45. It has been observed that the application of an electric field results in an increase in the band gap, consequently causing an optical blueshift in interband optical transitions along the armchair direction. Due to the prevalence of this topic in existing literature, we have chosen not to reiterate it in the current study.

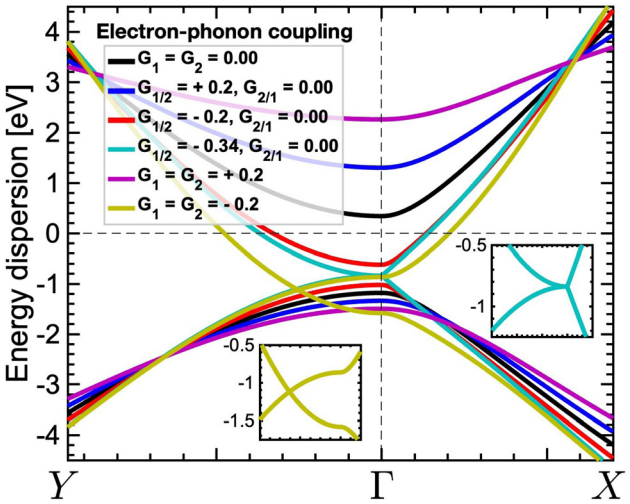

Fig. 2 The electronic band structure of phosphorene in the absence (presence) of an EF (EPC) is depicted along the directions Γ–X and Γ–Y. EPCs are expressed in units of eV. The Fermi energy level, represented by the black dashed horizontal line, remains fixed at zero. The band gap increases (decreases) with $G_{1/2} > 0$ ($G_{1/2} < 0$) and $G_{2/1} = 0$ and it is closed at $G_{1/2} = -0.34$ eV and $G_{2/1} = 0$. For $G_1 = G_2 > 0$, the band gap substantially increases, while for $G_1 = G_2 < 0$, a Dirac-like gap appears at finite momentum.

In Fig. 2, we plot the dispersion energy along the path Γ–X and Γ–Y of the FBZ of monolayer phosphorene. The plot reveals a high anisotropicity for the band structure along different paths, consistent with findings in ref. 37. Around the Γ point, a band gap of 1.52 eV is formed. Let us show the influence of the EPCs on the band gap in the absence of an EF. Evidently, the band gap in monolayer phosphorene increases with $G_{1/2} > 0$ and $G_{2/1} = 0$, *i.e.*, when only one of the sublayers is affected by the EPC, indicating a larger range of energy levels available to electrons in the material. This, in turn, introduces a configuration where the hybridized orbitals of host atoms have larger energy differences between them.

In instances where $G_{1/2} < 0$ and $G_{2/1} = 0$, the band gap experiences a reduction, indicating a narrowing of the energy range accessible to electrons. Simultaneously, the system transforms into a hole-doped semiconductor, with the gap located on the valence side. Notably, our analysis reveals that the difference between positive and negative energy dispersions in eqn (7) becomes zero at the Γ point under the condition:

$$2\tilde{t}_1 + \tilde{t}_2 + 2\tilde{t}_3 + \tilde{t}_5 = 0. \quad (15)$$

Using eqn (4), this condition yields $G_{1/2} \approx -0.34$ eV at $G_{2/1} = 0$. Accordingly, the band gap in the hole-doped semiconducting phase closes at this critical EPC strength, as illustrated by the light green line in Fig. 2.

When both sublayers are influenced by EPC effects and $G_1 = G > 0$, the band gap substantially increases (depicted by the yellow line in Fig. 2). In contrast, for $G_1 = G_2 < 0$, unlike other configurations, both the momentum and energy of

electrons shift to the y direction. Given that the momentum space of the FBZ is characterized by wave vectors associated with electron motion, this new phase of matter represents a crucial phenomenon for describing electronic transport in phosphorene. To determine the new momentum along the y direction where this phase emerges, we set $k_x = 0$ and $k_y \neq 0$ in eqn (6b), resulting in:

$$k_y^c = \frac{2\arccos[(\tilde{t}_2 + \tilde{t}_5)/2(\tilde{t}_1 + \tilde{t}_3)]}{b}, \quad (16)$$

The energy level of this phase appears to be somewhat independent of EPC strengths, while its momentum strongly depends on the values of G_1 and G_2. It is worth noting that for $G_{1/2} > G_{2/1}$ with positive EPCs, similar phenomena are observed as in the case of $G_{1/2} > 0$ and $G_{2/1} = 0$ or $G_1 = G_2 > 0$, each with different gap sizes. Also, for $G_{1/2} > G_{2/1}$ with negative EPCs, the results align with those of $G_{1/2} < 0$ and $G_{2/1} = 0$ or $G_1 = G_2 < 0$, again each with different gap sizes.

These variations in the band gap affect the optical absorption, a concept that will be explored further in the following discussions. Moving forward, we present the optical absorption of phosphorene with EPC. It is essential to note that all constants are set to unity such that an arbitrary unit is chosen. Results are plotted against the incident light frequency in the range of 0 eV $\leq \hbar\omega \leq$ 10 eV to cover the whole bandwidth shown in Fig. 2, with and without EF and EPC. The study here does not delve into the temperature dependence of the absorption, justified by the significant band gap of phosphorene, which far exceeds the thermal energy k_BT such that it remains largely unaffected by temperature, at least up to 300 K, corresponding to approximately 0.026 eV.

We start with the optical absorption of pristine phosphorene in the absence of an EF at $T = 10$ K. Given that the model is applicable to the low-energy range of bands, our attention is directed towards electronic excitations at low temperatures, with the phononic effects attributed to temperature being disregarded. This decision is justified by the simplicity of the tight-binding interaction terms in our Hamiltonian model. The absorption spectrum depicted in Fig. 3 varies for the armchair and zigzag paths, reflecting the inherent anisotropic nature of

Table 1 An overview of the responses of the electronic band structure and optical absorption to the electron–phonon coupling (EPC) to confirm the strongly anisotropic electro-optical properties of phosphorene

Parameter	Positive EPC	Negative EPC
Band gap	Increases	Decreases
Armchair peak	Red- and blue-shift	Red- and blue-shift
Zigzag peak	Redshift	Blueshift

phosphorene. The phosphorene's electronic dispersion in Fig. 2 reveals the presence of two distinct bands separated by a band gap in different paths. For phosphorene in the absence of doping (*i.e.*, $\mu = 0$ eV), there exists a singular transition between $\mathscr{E}_{\vec{k},+}$ and $\mathscr{E}_{\vec{k},-}$ in both directions at $\vec{k} = 0$, featuring two types of transitions – the first corresponding to the lowest peak ($\hbar\omega \simeq 1.52$ eV) and the second associated with $\hbar\omega \simeq 8.5$ eV in the armchair edge. Interestingly, a similar transition occurs at $\hbar\omega \simeq 7.5$ eV along the zigzag edge, and there is no minimal transition at low light frequencies, see black lines in Fig. 3. For $\hbar\omega > 8.5$ eV, according to Fig. 2, no bands appear, thus, optical absorption approaches zero independent of the direction. The emergence of the second transition along the armchair direction and the absence of such transition along the zigzag axis can be attributed to the electron and hole effective masses along these directions in phosphorene. Specifically, the effective masses in the vicinity of the Γ point are $m^{\mathrm{h}}_{\mathrm{armchair}} = 0.184m_{\mathrm{e}}$, $m^{\mathrm{e}}_{\mathrm{armchair}} = 0.167m_{\mathrm{e}}$, $m^{\mathrm{h}}_{\mathrm{zigzag}} = 1.143m_{\mathrm{e}}$, and $m^{\mathrm{e}}_{\mathrm{zigzag}} = 0.849m_{\mathrm{e}}$[37] ($m_{\mathrm{e}}$ denoting the bare electron mass). These values, along with eqn (9), highlight that electrons' and holes' transitions along the armchair direction, proportional to the difference between bands, are more facile than the zigzag path, particularly at large photon energies.

Let us turn to the influence of EPC on the directional-dependent optical absorption spectrum. When EPC is introduced, as its impact on the electronic band gap became a key factor, a shift in the position of the optical absorption peaks along both the armchair and zigzag directions is expected, as illustrated in Fig. 3. Specifically along the armchair direction in Fig. 3(a), the two peaks observed in the pristine phosphorene spectrum come into close proximity for positive values of the

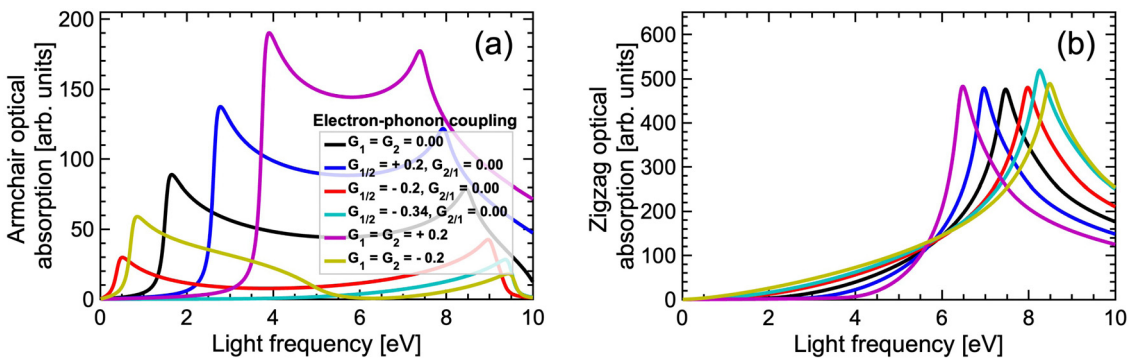

Fig. 3 The optical absorption of monolayer phosphorene in the absence (presence) of an EF (EPC) along the (a) armchair and (b) zigzag directions. In the zigzag direction, a redshift (blueshift) spectrum occurs with positive (negative) EPC, while both shifts are observed along the armchair direction, regardless of the sign of EPC.

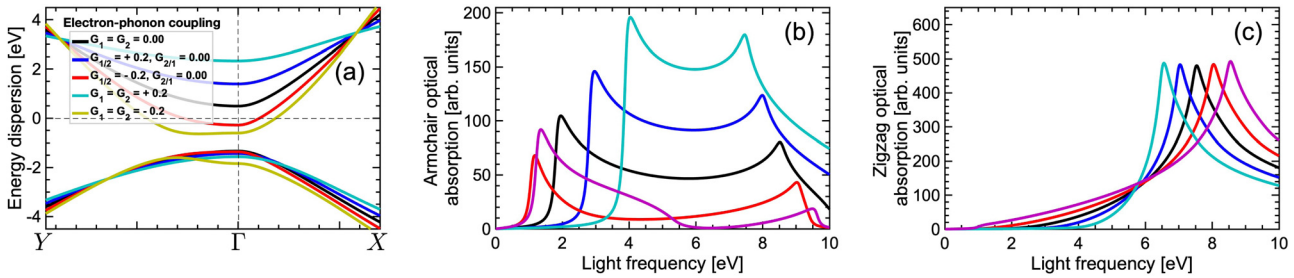

Fig. 4 (a) The electronic band structure and the optical absorption along the (b) armchair and (c) zigzag directions of phosphorene in the presence of both an EF and EPC. A strong (weak) blueshift is observed along the armchair (zigzag) direction as the EF is considered.

EPC parameter ($G > 0$). This proximity induces a blueshift in the spectrum for the first peak and a redshift for the second peak. By contrast, for negative values of G, except for the specific case of $G_{1/2} = -0.34$ eV and $G_{2/1} = 0$, the peaks move farther apart. In the critical case of $G_{1/2} = -0.34$ eV and $G_{2/1} = 0$, only a single blue peak appears at a light frequency of 9.5 eV, as a consequence of the zero band gap and the emergence of a hole-doped semiconducting phase, as elaborated earlier in the electronic dispersion of electrons. In Fig. 3(b), the optical absorption spectrum along the zigzag direction is characterized by a single peak. Interestingly, this peak exhibits distinctive behaviors for different values of the EPC parameter (G) compared to the peaks of the armchair direction. When G takes negative values ($G < 0$), the optical absorption peak experiences a blueshift. This means that the peak shifts toward shorter wavelengths or higher frequencies. For positive values of G ($G > 0$), the peak undergoes a redshift. In this case, the peak shifts toward longer wavelengths or lower frequencies. It is noteworthy that these shifts occur independently of the specific values of the EPC parameters.

Beyond the shifts observed, the peak heights along both directions change significantly. A plausible explanation for the observed increase (decrease) in the peak magnitude of optical absorption with $G > 0$ ($G < 0$) can be inferred from the broadening (narrowing) of the band structure. As the level of broadening and narrowing are different for two directions, the change rates for the height of peaks are different.

A summary of the EPC effects on the electronic band gap and optical absorption is shown in Table 1. It is evident that phosphorene is highly anisotropic.

When a gate voltage is applied at a given temperature, for example at $T = 10$ K, to both sublayers with $+\Delta_z/2$ and $-\Delta_z/2$, the band gap undergoes an increase from 1.52 eV to 2 eV for $\Delta_z = 1$ eV, as depicted with the dark gray line in Fig. 4(a). It is important to note that both sublayers are gated at the same time in our model with different signs. Thus, $\Delta_z \mapsto -\Delta_z$ does not change the results. In the presence of EPC, if only one of the sublayers is influenced by the EPC, we find an increase (a decrease) of the band gap with $G > 0$ ($G < 0$). Although in contrast to the ungated lattice, the band gap never closes meaning that there is no critical EPC at which the valence and conduction bands touch each other, the shift of the momentum space still occurs following $k_y^c = \frac{2\arccos[((\Delta_z/2) - (\tilde{t}_2 + \tilde{t}_5)/2(\tilde{t}_1 + \tilde{t}_3))]}{b}$.

With the EF, the distinction between results, compared to the absence of an EF, along the armchair and zigzag directions is quite different such that the optical peaks are significantly (slightly) shifted to the higher light frequencies along the armchair (zigzag) direction, as illustrated in Fig. 4(b) and (c). This implies that gate voltages exhibit distinct effects along the x and y directions in monolayer phosphorene, a crucial aspect for optoelectronics.

5 Summary

To sum up, our investigation focuses on the theoretical model of interband optical responses in single-layer black phosphorus under the influence of electron–phonon coupling (EPC) and an electric field (EF). Utilizing the effective tight-binding Hamiltonian model based on the Barišic–Labbe–Friedel–Su–Schrieffer–Heeger model and the Kubo formalism, we calculate the direction-dependent electronic band structure and optical absorption. The normalization of orbital hybridization through EPC is manifested in the opening/closing of the band gap. EPC induces blue and redshifts in the optical absorption spectrum along both directions depending on the sign of EPC. Our findings with EPC remain relatively stable in the presence of an EF. The present findings provide valuable insights for the adjustment of phosphorene's optoelectronic applications.

Conflicts of interest

There are no conflicts to declare.

Acknowledgements

This research is funded by University of Education, Hue University under grant number T.23-TN.SV-02.

References

1 K. S. Novoselov, A. K. Geim, S. V. Morozov, D. Jiang, Y. Zhang and S. V. Dubonos, *et al.*, Electric Field Effect in Atomically Thin Carbon Films, *Science*, 2004, **306**(5696), 666–669, https://www.science.org/doi/abs/10.1126/science.1102896.

2 K. S. Novoselov, A. K. Geim, S. V. Morozov, D. Jiang, M. I. Katsnelson and I. V. Grigorieva, *et al.*, Two-dimensional gas of massless Dirac fermions in graphene, *Nature*, 2005, **438**(7065), 197–200, **https://www.nature.com/articles/nature04233#citeas**.

3 K. S. Novoselov, Z. Jiang, Y. Zhang, S. V. Morozov, H. L. Stormer and U. Zeitler, *et al.*, Room-Temperature Quantum Hall Effect in Graphene, *Science*, 2007, **315**(5817), 1379, **https://www.science.org/doi/abs/10.1126/science.1137201**.

4 A. H. Castro Neto, F. Guinea, N. M. R. Peres, K. S. Novoselov and A. K. Geim, The electronic properties of graphene, *Rev. Mod. Phys.*, 2009, **81**, 109–162, **https://link.aps.org/doi/10.1103/RevModPhys.81.109**.

5 F. Schwierz, The electronic properties of graphene, *Nat. Nanotechnol.*, 2010, **5**, 487–496, DOI: **10.1038/nnano.2010.89**.

6 J. Sone, T. Yamagami, Y. Aoki, K. Nakatsuji and H. Hirayama, Epitaxial growth of silicene on ultra-thin Ag(111) films, *New J. Phys.*, 2014, **16**(9), 095004, DOI: **10.1088/1367-2630/16/9/095004**.

7 M. E. Dávila, L. Xian, S. Cahangirov, A. Rubio and G. L. Lay, Germanene: a novel two-dimensional germanium allotrope akin to graphene and silicene, *New J. Phys.*, 2014, **16**(9), 095002, DOI: **10.1088/1367-2630/16/9/095002**.

8 V. Wang, Y. Kawazoe and W. T. Geng, Native point defects in few-layer phosphorene, *Phys. Rev. B: Condens. Matter Mater. Phys.*, 2015, **91**, 045433, **https://link.aps.org/doi/10.1103/PhysRevB.91.045433**.

9 B. Radisavljevic, A. Radenovic, J. Brivio, V. Giacometti and A. Kis, Single-layer MoS2 transistors, *Nat. Nanotechnol.*, 2011, **6**, 147–150, DOI: **10.1038/nnano.2010.279**.

10 H. Fang, S. Chuang, T. C. Chang, K. Takei, T. Takahashi and A. Javey, High-Performance Single Layered WSe2 p-FETs with Chemically Doped Contacts, *Nano Lett.*, 2012, **12**(7), 3788–3792, DOI: **10.1021/nl301702r**.

11 V. Tran, R. Soklaski, Y. Liang and L. Yang, Layer-controlled band gap and anisotropic excitons in few-layer black phosphorus, *Phys. Rev. B: Condens. Matter Mater. Phys.*, 2014, **89**, 235319, **https://link.aps.org/doi/10.1103/PhysRevB.89.235319**.

12 B. Sa, Y. L. Li, Z. Sun, J. Qi, C. Wen and B. Wu, The electronic origin of shear-induced direct to indirect gap transition and anisotropy diminution in phosphorene, *Nanotechnology*, 2015, **26**(21), 215205, DOI: **10.1088/0957-4484/26/21/215205**.

13 L. Li, Y. Yu, G. J. Ye, Q. Ge, X. Ou and H. Wu, *et al.*, Black phosphorus field-effect transistors, *Nat. Nanotechnol.*, 2014, **9**, 372–377, DOI: **10.1038/nnano.2014.35**.

14 F. Xia, H. Wang and Y. Jia, Rediscovering black phosphorus as an anisotropic layered material for optoelectronics and electronics, *Nat. Commun.*, 2014, **5**, 4458, DOI: **10.1038/ncomms5458**.

15 S. P. Koenig, R. A. Doganov, H. Schmidt, A. H. Castro Neto and B. Özyilmaz, Electric field effect in ultrathin black phosphorus, *Appl. Phys. Lett.*, 2014, **104**(10), 103106, DOI: **10.1063/1.4868132**.

16 G. Zhang, S. Huang, F. Wang, Q. Xing, C. Song and C. Wang, *et al.*, The optical conductivity of few-layer black phosphorus by infrared spectroscopy, *Nat. Commun.*, 2020, **11**, 1847, DOI: **10.1038/s41467-020-15699-7**.

17 J. Yang and Y. Lu, Optical properties of phosphorene, *Chin. Phys. B*, 2017, **26**(3), 034201, DOI: **10.1088/1674-1056/26/3/034201**.

18 T. Low, R. Roldán, H. Wang, F. Xia, P. Avouris and L. M. Moreno, *et al.*, Plasmons and Screening in Monolayer and Multilayer Black Phosphorus, *Phys. Rev. Lett.*, 2014, **113**, 106802, **https://link.aps.org/doi/10.1103/PhysRevLett.113.106802**.

19 J. Qiao, X. Kong, Z. X. Hu, F. Yang and W. Ji, High-mobility transport anisotropy and linear dichroism in few-layer black phosphorus, *Nat. Commun.*, 2014, **5**, 4475, DOI: **10.1038/ncomms5475**.

20 M. Buscema, D. J. Groenendijk, S. I. Blanter, G. A. Steele, H. S. J. van der Zant and A. Castellanos-Gomez, Fast and Broadband Photoresponse of Few-Layer Black Phosphorus Field-Effect Transistors, *Nano Lett.*, 2014, **14**(6), 3347–3352, DOI: **10.1021/nl5008085**.

21 T. Low, A. S. Rodin, A. Carvalho, Y. Jiang, H. Wang and F. Xia, *et al.*, Tunable optical properties of multilayer black phosphorus thin films, *Phys. Rev. B: Condens. Matter Mater. Phys.*, 2014, **90**, 075434, **https://link.aps.org/doi/10.1103/PhysRevB.90.075434**.

22 N. Youngblood, C. Chen, S. J. Koester and M. Li, Waveguide-integrated black phosphorus photodetector with high responsivity and low dark current, *Nat. Photonics*, 2015, **9**, 247–252, DOI: **10.1038/nphoton.2015.23**.

23 Zhang X. Huang Ly, M. Zhang and G. Lu, Optically inactive defects in monolayer and bilayer phosphorene: A first-principles study, *Phys. Rev. Mater.*, 2018, **2**, 054003, **https://link.aps.org/doi/10.1103/PhysRevMaterials.2.054003**.

24 Z. Torbatian and R. Asgari, Optical absorption properties of few-layer phosphorene, *Phys. Rev. B.*, 2018, **98**, 205407, **https://link.aps.org/doi/10.1103/PhysRevB.98.205407**.

25 L. L. Li, B. Partoens, W. Xu and F. M. Peeters, Electric-field modulation of linear dichroism and Faraday rotation in few-layer phosphorene, *2D Mater.*, 2018, **6**(1), 015032, DOI: **10.1088/2053-1583/aaf47f**.

26 A. N. Rudenko, S. Yuan and M. I. Katsnelson, Toward a realistic description of multilayer black phosphorus: From GW approximation to large-scale tight-binding simulations, *Phys. Rev. B: Condens. Matter Mater. Phys.*, 2015, **92**, 085419, **https://link.aps.org/doi/10.1103/PhysRevB.92.085419**.

27 Y. Jiang, R. Roldán, F. Guinea and T. Low, Magnetoelectronic properties of multilayer black phosphorus, *Phys. Rev. B: Condens. Matter Mater. Phys.*, 2015, **92**, 085408, **https://link.aps.org/doi/10.1103/PhysRevB.92.085408**.

28 C. Lin, R. Grassi, T. Low and A. S. Helmy, Multilayer Black Phosphorus as a Versatile Mid-Infrared Electro-optic Material, *Nano Lett.*, 2016, **16**(3), 1683–1689, DOI: **10.1021/acs.nanolett.5b04594**.

29 S. Saberi-Pouya, T. Vazifehshenas, T. Salavati-fard, M. Farmanbar and F. M. Peeters, Strong anisotropic optical

conductivity in two-dimensional puckered structures: The role of the Rashba effect, *Phys. Rev. B*, 2017, **96**, 075411, https://link.aps.org/doi/10.1103/PhysRevB.96.075411.

30 M. Tahir, P. Vasilopoulos and F. M. Peeters, Magneto-optical transport properties of monolayer phosphorene, *Phys. Rev. B: Condens. Matter Mater. Phys.*, 2015, **92**, 045420, https://link.aps.org/doi/10.1103/PhysRevB.92.045420.

31 R. D. Çakir, H. Sahin and F. M. Peeters, Tuning of the electronic and optical properties of single-layer black phosphorus by strain, *Phys. Rev. B: Condens. Matter Mater. Phys.*, 2014, **90**, 205421, https://link.aps.org/doi/10.1103/PhysRevB.90.205421.

32 M. Yarmohammadi, B. D. Hoi and L. T. T. Phuong, Systematic competition between strain and electric field stimuli in tuning EELS of phosphorene, *Sci. Rep.*, 2021, **11**, 3716, DOI: 10.1038/s41598-021-83213-0.

33 M. Yarmohammadi, M. M. Nobahari, T. S. Tien and L. T. T. Phuong, Linear interband optical refraction and absorption in strained black phosphorene, *J. Phys.: Condens. Matter*, 2020, **32**(46), 465301, DOI: 10.1088/1361-648X/abaad0.

34 L. T. T. Phuong, T. C. Phong and M. Yarmohammadi, Spin-splitting effects on the interband optical conductivity and activity of phosphorene, *Sci. Rep.*, 2020, **10**, 9201, DOI: 10.1038/s41598-020-65951-9.

35 Y. Yin, X. Zhao, X. Ren, K. Liu, J. Zhao and L. Zhang, *et al.*, Thickness Dependent Ultrafast Charge Transfer in BP/MoS2 Heterostructure, *Adv. Funct. Mater.*, 2022, **32**(45), 2206952, https://onlinelibrary.wiley.com/doi/abs/10.1002/adfm.202206952.

36 L. Zhang, W. Chu, Q. Zheng, A. V. Benderskii, O. V. Prezhdo and J. Zhao, Suppression of Electron-Hole Recombination by Intrinsic Defects in 2D Monoelemental Material, *J. Phys. Chem. Lett.*, 2019, **10**(20), 6151–6158, DOI: 10.1021/acs.jpclett.9b02620.

37 S. Yuan, A. N. Rudenko and M. I. Katsnelson, Transport and optical properties of single- and bilayer black phosphorus with defects, *Phys. Rev. B: Condens. Matter Mater. Phys.*, 2015, **91**, 115436, https://link.aps.org/doi/10.1103/PhysRevB.91.115436.

38 M. Ezawa, Topological origin of quasi-flat edge band in phosphorene, *New J. Phys.*, 2014, **16**(11), 115004, DOI: 10.1088/1367-2630/16/11/115004.

39 A. N. Rudenko and M. I. Katsnelson, Quasiparticle band structure and tight-binding model for single- and bilayer black phosphorus, *Phys. Rev. B: Condens. Matter Mater. Phys.*, 2014, **89**, 201408, https://link.aps.org/doi/10.1103/PhysRevB.89.201408.

40 G. Q. Huang and Z. W. Xing, Superconductivity of bilayer phosphorene under interlayer compression, *Chin. Phys. B*, 2016, **25**, 027402, https://cpb.iphy.ac.cn/article/2016/1809/cpb_25_2_027402.html.

41 D. J. P. de Sousa, L. V. de Castro, D. R. da Costa, J. M. Pereira and T. Low, Multilayered black phosphorus: From a tight-binding to a continuum description, *Phys. Rev. B.*, 2017, **96**, 155427, https://link.aps.org/doi/10.1103/PhysRevB.96.155427.

42 C. H. Yang, J. Y. Zhang, G. X. Wang and C. Zhang, Dependence of the optical conductivity on the uniaxial and biaxial strains in black phosphorene, *Phys. Rev. B*, 2018, **97**, 245408, https://link.aps.org/doi/10=1103/PhysRevB.97.245408.

43 J. M. Galicia Hernandez, H. N. Fernandez-Escamilla, J. Guerrero Sanchez and N. Takeuchi, Electronic and optical properties of the buckled and puckered phases of phosphorene and arsenene, *Sci. Rep.*, 2022, **12**, 20979, DOI: 10.1038/s41598-022-24425-w.

44 J. Yang, R. Xu, J. Pei, Y. W. Myint, F. Wang and Z. Wang, *et al.*, Optical tuning of exciton and trion emissions in monolayer phosphorene, *Light: Sci. Appl.*, 2015, **4**, e312–e312, DOI: 10.1038/lsa.2015.85.

45 K. D. Pham, N. N. Hieu, M. Davoudiniya, L. T. T. Phuong, B. D. Hoi and C. V. Nguyen, *et al.*, Electric field tuning of dynamical dielectric function in phosphorene, *Chem. Phys. Lett.*, 2019, **731**, 136606, https://www.sciencedirect.com/science/article/pii/S0009261419305780.

46 S. Barišić, J. Labbé and J. Friedel, Tight Binding and Transition-Metal Superconductivity, *Phys. Rev. Lett.*, 1970, **25**, 919–922, https://link.aps.org/doi/10.1103/PhysRevLett.25.919.

47 S. Barišić, Rigid-Atom Electron-Phonon Coupling in the Tight-Binding Approximation.I, *Phys. Rev. B: Solid State*, 1972, **5**, 932–941, https://link.aps.org/doi/10.1103/PhysRevB.5.932.

48 S. Barišić, Self-Consistent Electron-Phonon Coupling in the Tight-Binding Approximation. II, *Phys. Rev. B: Solid State*, 1972, **5**, 941–951, https://link.aps.org/doi/10.1103/PhysRevB.5.941.

49 W. P. Su, J. R. Schrieffer and A. J. Heeger, Solitons in Polyacetylene, *Phys. Rev. Lett.*, 1979, **42**, 1698–1701, https://link.aps.org/doi/10.1103/PhysRevLett.42.1698.

50 V. D. Neverov, A. E. Lukyanov, Y. V. Zhumagulov, A. V. Krasavin and V. Perebeinos, Polaronic signatures in pristine phosphorene, *Phys. Rev. Mater.*, 2021, **5**, 054008, https://link.aps.org/doi/10.1103/PhysRevMaterials.5.054008.

51 R. Kubo, Statistical-Mechanical Theory of Irreversible Processes. I. General Theory and Simple Applications to Magnetic and Conduction Problems, *J. Phys. Soc. Jpn.*, 1957, **12**(6), 570–586, DOI: 10.1143/JPSJ.12.570.

52 G. D. Mahan, *Many-Particle Physics, Physics of Solids and Liquids*, Springer New York, NY, 2000, DOI: 10.1007/978-1-4757-5714-9.

53 G. Grosso and G. P. Parravicini, *Solid State Physics*, Academic Press, NY, 2014, DOI: 10.1016/C2010-0-66724-1.

